v. 2, n. 24, 2022

Journal of
Engineering
Research

HYDROTHERMAL SYNTHESIS OF COPPER II-DOPED TITANATES FROM DOPED PRECURSORS

Felipe Moessa Bezerra

Daniela Cristina Manfroi Rodrigues

Wilson Soares Dos Reis Filho

Fabrícia Emanueli Moreira Dias

Alberto Adriano Cavalheiro

Ademir dos Anjos

Rony Gonçalves de Oliveira

Guilhermina Ferreira Teixeira

INTRODUCTION

In addition to increasing the shelf life of food is a topic that has been gaining attention from the food industry, and avoiding its contamination by microorganisms that cause degradation and loss of the product is one of the ways.

In this sense, transition metal oxides can be great allies, especially titanium oxide, due to its versatility of applications, which includes the medicinal, environmental, energy aspects, among others. Titanium oxide, when irradiated with light, has the ability to oxidize/reduce molecules present in water and also in air, and this ability is widely used to remove various toxic substances from these environments[1]. In semiconductors used in photocatalysis, the electronic excitation process can be activated by light.

After irradiation of titanium dioxide (TiO2) with UV light, reactive oxygen species such as hydrogen peroxide, superoxide radical and hydroxyl radicals are generated. Bacterial cell membranes and viral capsule proteins are attacked by these species, causing the bacteria to die and the viruses to inactivation. And this is even reported for drug-resistant microorganisms, such as gram-positive bacteria (Methicillin Resistant Staphylococcus aureus, Vancomycin Resistant Enterococcus faecalis and Penicillin Resistant Streptococcus pneumoniae), gram-negative bacteria (Escherichia coli and Pseudomonas aeruginosa multiresistant), and influenza virus, which makes this material highly attractive[2].

Photocatalytic disinfection using this material against fungi, viruses[3] and bacteria[4] is a process that is already commercially available and occurs by a mechanism very similar to the one described above[5]. This biocidal capacity of the material can be increased with the presence of metallic dopants such as silver and copper[6].

The structure that covers the bacterium Escherichia coli is passive to being attacked by these reactive species, thus causing the death of the cells. It is also worth mentioning that the inactivation of these organisms depends on their interaction with the surface of the material, in which the reactive species are found, therefore, the choice of a suitable material for this use must be made in function of a greater availability of surface area, where the sites responsible for the reactions are located.

The photocatalytic action, both for the removal of dyes and for the inactivation of microorganisms, of this material depends on the generation of reactive oxygen species on the surface, formed through reduction and oxidation reactions, whose products attack the organic components of the surface. cell causing its inactivity[5].

Titanium oxide with nanotube morphology is easily obtained through the hydrothermal method[7], which is based on heating a closed system, which contains a mineralizing solution and the reagents. As the temperature increases, the internal pressure of the system also increases. The reaction of transforming reactants into products is governed by the mechanism of dissolution-reprecipitation, of reactants into products, which occurs dynamically as long as heat and reactants are available. These materials have high surface area, structures about 10 nm wide by several micrometers in length[8].

As it is a very versatile method, several reports of structural modification are found in the literature. Most are based on chemical and heat treatments after hydrothermal synthesis.

This work aimed to carry out the synthesis of copper-doped precursors using the polymeric precursors method and use these samples to, through hydrothermal treatment, produce nanostructures of titanates and test their photocatalytic efficiency in removing

the dye (methylene blue) and to inhibit the formation of microorganisms, responsible for food degradation.

METHODOLOGY

SYNTHESIS OF PRECURSORS

Synthesis of Titanium IV Resin: Citric acid was dissolved under stirring in isopropanol, then titanium isopropoxide and distilled water were added, the mixture was heated until the isopropoxide dissolved. After evaporation of the isopropanol, the ethylene glycol was added under heating until the viscosity was reached. The ratio of citric acid: titanium isopropoxide: ethylene glycol used was 2.5 mol:1 mol:5 mol.

Doping of Titanium IV Resin with Copper II: The mass of CuCl2 to add to the titanium IV resin was calculated to form the precursor TiO2-Cu5% w/w. For the homogenization of the mixture, about 250 mL of water was added to the Ti4+ resin, followed by the addition of copper II, and left under magnetic stirring for 1 hour.

Heat treatment: Titanium IV resins and copper II doped resin were taken separately for calcination at 350 °C for 4 hours. Then, the coals formed were crushed for 1 hour with isopropyl alcohol, taking them again to calcination at 500 °C for 2 hours. After that, it was triturated again using isopropyl alcohol. The final product presented a white color, respectively, being named as TiO2–350–500 ºC (Figure 1a) and moss green coloring, named as TiO2-Cu–350–500 ºC (Figure 1b).

Figure 1

HYDROTHERMAL SYNTHESIS OF NANOPARTICLES

Two syntheses were performed separately using the samples TiO2-350-500 ºC and TiO2-Cu-350-500 as precursors, both following the same procedure. In a Teflon® and stainless steel reactor, 50 mL of a 10 mol. L-1 sodium hydroxide solution and 0.5 g of one of the precursors were added. The temperature was set at 110 °C for 24 hours. The obtained samples named SH-MPP-TiO2-350-500 °C and SH-MPP-TiO2-350-500 °C-Cu were washed until pH = 7.0 and then dried at room temperature (Figure 2).

Figure 2

STRUCTURAL CHARACTERIZATION

Photoluminescence Spectroscopy: Performed in a Thermal JarrelAsh equipment, with a Monospec 27 monochromator and a Hamamatsu R446 photomultiplier, with an excitation 350 nm Krypton ion laser (CoherentInnova) maintaining the power at 550 mW.

X-Ray Diffractometry: Performed at the Universidade Estadual Paulista (UNESP), Araraquara-SP Unit. Samples were analyzed using a Rigaku Rotaflex diffractometer with rotating anode, model rint 2000 with Cu Kα radiation, in the range of 2θ 10 – 80°, with a step of 0.01°, monochromatized by graphite crystal.

Raman Spectroscopy: Performed with equipment equipped with a laser (530 nm green) positioned, through an optical microscope, on the surface of the Samples. A "probe" collects the Raman scattering signal and the operating system compiles the data. Scanning in the range of 50-1000 cm-1, with collection of 120s, adjusting the laser between 10-40 mV according to the best response of the Samples.

PHOTOCATALYSIS

Performed by discoloration control, using standardized dye solution (0.01 mmol. L-1 concentration of methylene blue) and photocatalyst (0.1 g. L-1 concentration) under UV-A and UV-C light to activate the materials. Procedure performed for all Samples obtained in the precursor syntheses (MPP–TiO2– 350-500, MPP–TiO2–350-500–Cu II, SH-MPP-TiO2-350-500 ºC and SH-

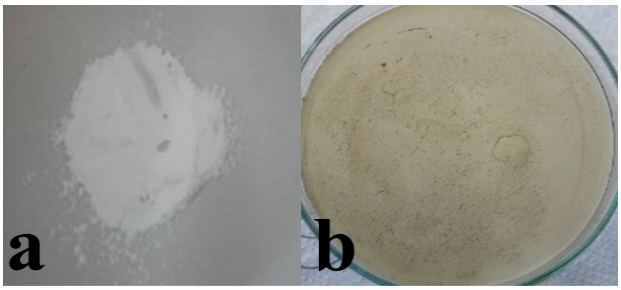

Figure 1 - (a) Sample TiO2–350–500 ºC and (b) Sample TiO2–Cu-350-500 ºC.

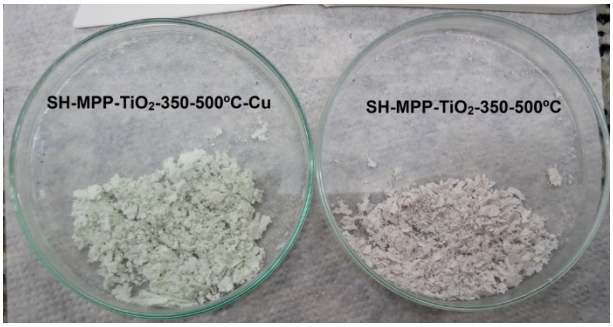

Figure 2 - Dried samples (SH-MPP-TiO2-350-500 ºC and SH-MPP-TiO2-350-500 ºC-Cu), after hydrothermal synthesis.

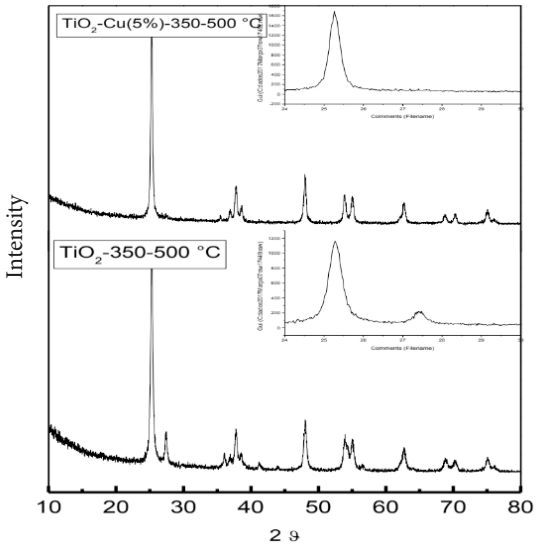

Figure 3 - X-Ray Diffractograms of Samples synthesized via the Polymeric Precursors Method and heat treated in two stages.

MPP-TiO2-350-500 ºC-Cu. Then the aliquots were submitted to UV-visible spectroscopic analysis, carried out at the State University of Mato Grosso do Sul (UEMS), using the Varian Cary 50 equipment, quartz cuvette, and slow scanning speed in the range of 200-800 nm.

ANTIMICROBIAL TESTS

This assay was performed by the disk diffusion method on Agar. For antimicrobial evaluations, Staphylococcus aureus (CCCD-5007), Enterococcus faecalis (CCCD-E002), Pseudomonas aeroginosis (CCCD-P003), Escherichia Coli (CCCD - E009) and Bacilus cereus (CCCD-B001) bacteria were selected.

TiO2-based materials (MPP-TiO2-350-500, MPP-TiO2-350-500-Cu, SH-MPP-TiO2-350-500 and SH-MPP-TiO2-350-500-Cu) were immobilized in cellulose and subjected to an initial screening using the agar disk diffusion method, incubated at 35 °C for 24 hours under black light (UV-A) or UV-C light. After incubation, the existence of inhibition halos or any region of inhibition of bacterial growth was verified.

RESULTS AND DISCUSSION

STRUCTURAL CHARACTERIZATION OF PRECURSORS

It was observed (Figure 3) that the TiO2 sample-350-500 ºC showed peaks at 2θ= 25, 37, 48, 53, 55, 62 ° related to the anatase phase (PDF# 84-1285) and a peak at 2θ= 27° referring to the rutile phase (PDF # 77-441). By comparing the peak intensities at 2θ=25° and 2θ=27°, it is inferred that there is approximately 18% of rutile phase in the sample, that is, even carrying out a heat pre-treatment step to eliminate organic matter in excess, the formation of an amount of rutile phase occurs. This secondary phase does not appear in the diffractogram of the TiO2-Cu-350-500 ºC sample, which shows only the characteristic peaks of the anatase phase, indicating that the presence of copper in the sample, which underwent the same types of heat treatment, favors crystallization. of the anatase structure.

Figure 3

From the "width at half height" data, it was possible to use the Scherrer equation[9] to calculate crystallite size parameters:

$$\beta = \frac{k\,D}{\lambda \cos\theta} \;\rightarrow\; D = \frac{k\,\lambda}{\beta\,\cos\theta} \qquad (1)$$

Where:

D: Crystallite size; k: constant of form, in this case k = 0.9; λ: x-ray wavelength; β: width at half height (FWHM) e θ: Bragg angle.

It was also assumed that the peak broadening is a result of lattice microstrain, expressed as:

$$\beta = 2.\varepsilon.tan\theta \qquad (2)$$

Where ε is the lattice microstrain (network voltage)[10].

Using the Scherrer equation, it was verified that for the pre-stage of heat treatment (350 °C for 4 hours) the anatase structure presented a crystallite size of 31.74 nm for TiO2-350-500 ºC (Table 1). After the insertion of copper ions in the polymeric resin, and after the heat treatment, in the crystal structure an increase in the size of the crystallites to 37.81 nm was observed, this was mainly due to the differences in ionic radii, since Ti4 + has a 0.60 Å which was replaced by the Cu2+ ion with a radius of 0.72 Å.

Table 1

In the Raman Spectrum of the Samples (Figure 4) it is possible to observe the presence of the main active modes related to the anatase structure, for the TiO2-350-500 sample, located at 146, 195, 396, 514 and 637 cm-1. For the copper sample (TiO2-Cu- 350-500-), the peak of 146 cm-1, related to the titanium atom in the center of the octahedron (TiO6), was shifted to 151 cm-1 indicating

I	Period	Composition	Size of C Crystallite	Mains Voltage
TiO_2-350-500 °C	Anatase (PDF# 84-1285)	81.24 %	31.74 nm	0.0052
	Rutile (PDF # 77-441)	18.76 %	29.88 nm	0.0051
TiO_2-350-500 °C-Cu(5%)	Anatase (PDF# 84-1285)	100 %	37.81 nm	0.0044

Table 1: Structural parameters, obtained from the Scherrer equation of the Samples.

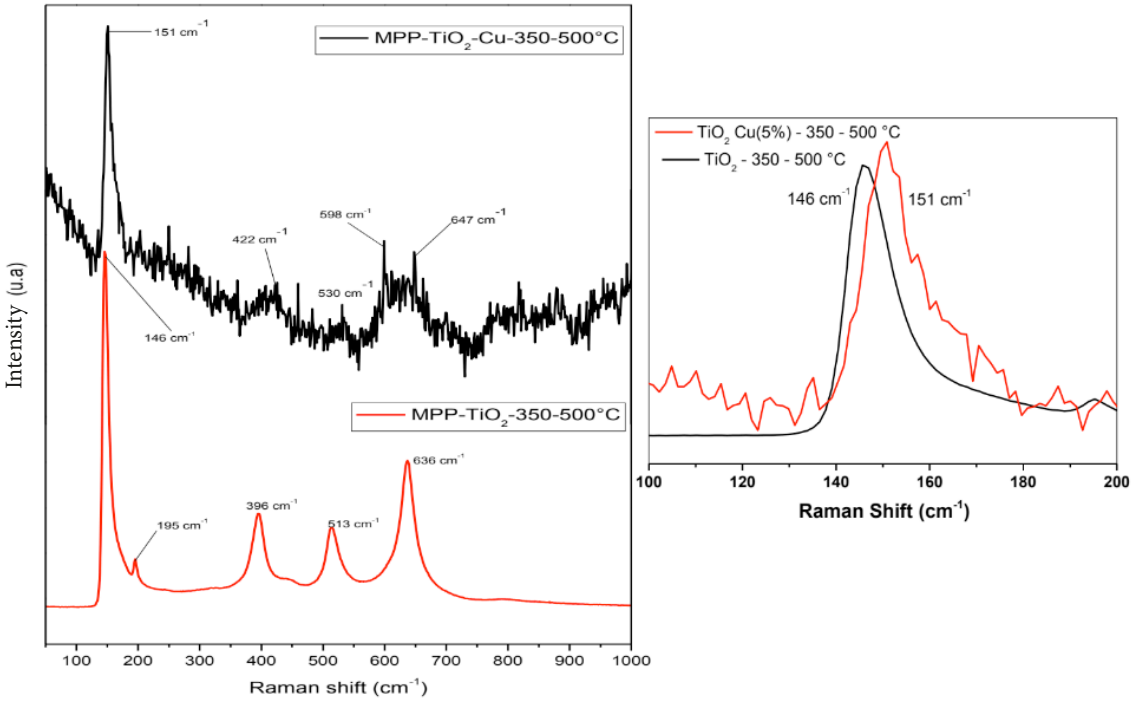

Figure 4 - Raman Spectrum of Samples obtained via the Polymeric Precursors Method and heat treated in two stages.

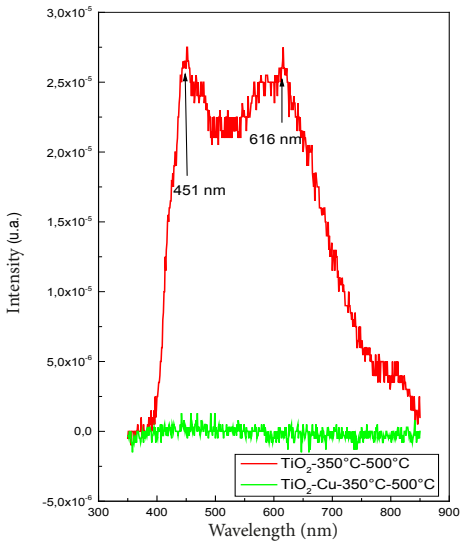

Figure 5 - Luminescence spectrum of the samples synthesized by the Polymeric Precursors Method, using a staggered heat treatment with two main stages: 350 °C for 4 hours and 500 °C for 2 hours.

that titanium was replaced by copper.

Figure 4

With photoluminescence spectroscopy (Figure 5) it was verified that the TiO2 sample–350–500 °C presented two main peaks at 451 nm (blue region of the visible spectrum) and 616 nm (orange region of the visible spectrum), which is the latter less energetic than the former. While for the TiO2-Cu–350–500 °C sample, it was not possible to distinguish any peak or emission band. Another characteristic of the spectra is the emission intensity indicating the concentration of structural defects (which are formed during the calcination process).

It can be seen that the TiO2-Cu–350–500 °C sample has a very low intensity, which leads to the inference that the presence of copper II in the crystalline structure leads to a better organization of this structure, not being possible, through this technique, infer about the presence of structural defects.

Figure 5

STRUCTURAL CHARACTERIZATION OF NANOPARTICLES

Figure 6 illustrates the diffractograms of Nanoparticle Samples obtained after hydrothermal synthesis at 110 °C for 24 hours. For both samples it was verified the set of peaks in the same positions 2θ= 10, 24, 28, 48 and 62°, with low intensity and widened. The peak around 2θ= 10° (note: the collection started at 2θ= 10° so it is not possible to verify its intensity and width at half height) can be identified with a "layered titanate" or lamellar structure, because this peak is characteristic of this type of diffraction between the layers.

This peak at 2θ= 10°, common in this type of structure, consists of layers of planes (1 0 0) referring to the TiO6 octahedrons that are distributed in a sinuous way through the structure, linked together through the edges, in structures that hold ions, and that can be exchanged, in the spaces between layers. The doping of these structures in layers through the ion exchange (of the ion Na+ or H+ intercalated in this space during the hydrothermal synthesis) is the most common methodology reported in the literature, however, this work is refers to observing the effect of replacing the Ti4+ ion in the center of the TiO6 octahedron by the Cu2+ ion. As the two observed diffractograms overlap and the peaks are wider and less intense, through the XRD technique, it was not possible to observe this substitution in the lattice parameters.

Figure 6

The specters show the presence of five main bands located at ~150, 194, 276, 440 and 699 cm-1. The band at 150 cm-1 can be associated with the TiO6 vibration of the oxygen octahedron, which is the basic unit forming anatase and present in the nanostructures, and the bands at ~270, 440, 700 cm−1 refer to the Ti- O-Ti of the crystal lattice11, 12.

In the black spectrum (SH-TiO2-Cu-350-500), there is a peak at 151 cm-1, which coincides with the same peak in figure 4, which is an indication that the copper II ion continues to occupy the center of the octahedron. There is also a shift, for a higher wave number, from the band at 436 cm-1 to 445 cm-1 for the sample containing copper, another indication of the Ti-O-Cu bond that would have formed in the crystal structure of the octahedra.

Figure 7

PHOTOCATALYTIC ACTIVITY

In the graph, it is possible to observe the action of the synthesized materials (precursors and nanoparticles) under the irradiation of UV-A light, less energetic radiation. The first graph (%Removal versus time) shows that Samples TiO2-350-500 and TiO2-Cu-350-500, which are the precursors of nanoparticles, showed removal efficiency

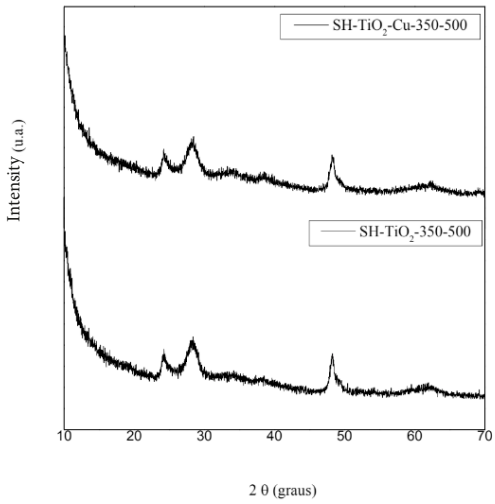

Figure 6 - X-Ray Diffractograms of Nanoparticle Samples, Post Hydrothermal Synthesis, SH-TiO_2-350-500 e SH-TiO_2-Cu-350-500.

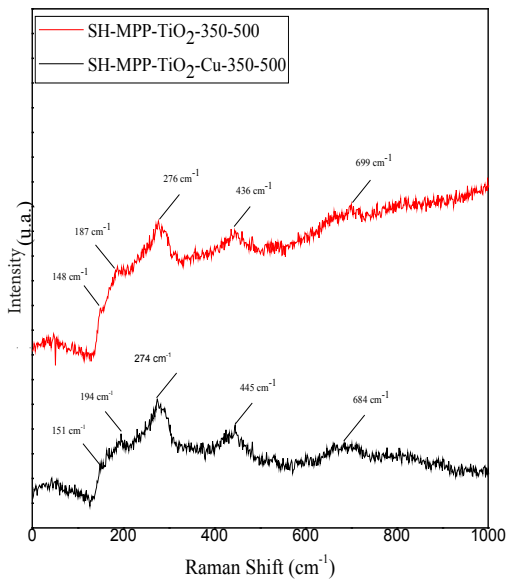

Figure 7 - Raman spectrum of nanostructures, obtained after Hydrothermal Synthesis, from Samples SH-TiO_2-350-500 e SH-TiO_2-350-500-Cu II.

of 32.2 and 6.6% in 60min, respectively.

For this irradiation energy, the copper-doped sample had a similar performance to photolysis, that is, little dye removal can be attributed to the adsorption and photocatalysis mechanisms of this sample. On the other hand, the samples of nanoparticles obtained, after the hydrothermal synthesis, showed an efficiency in the removal of the dye of 95.6 and 96.2% in 60min, for the Samples SH-TiO2-350-500 and SH-TiO2-Cu- 350-500, close values, and, for this irradiation condition, both had equivalent efficiency.

Figure 8

When we analyzed the *Figure 10*, we verified in the graph, %Removal versus time, that for all samples the use of irradiation of UV-C light increased the efficiency of removing methylene blue from the aqueous medium, with nanoparticles being the most efficient 95.5 and 99.3% for SH-TiO2-350-500 and SH-TiO2-Cu-350-500, respectively.

Figure 10

The photocatalytic discoloration of dyes, using solid catalysts, can be described by the Langmuir–Hinshelwood kinetic model, noting that this is a standard model. . In this study, the Langmuir–Hinshelwood model (pseudo first order) was used to investigate the kinetic parameters of methylene blue dye discoloration using the precursors and nanoparticles. The equation describing the model is as follows:

$$ln\frac{A}{A_0} = -kt \qquad (3)$$

The *Figure 8* and *Figure* 10 show the graphs obtained from the linearization of the data using this model and Table 2 summarizes these parameters. Through this it is verified that all the adjustments (R2) can be considered good, since they have values greater than 0.78.

When compared to the other materials, the precursor doped with Cu2+ in UV-A and UV-C lights showed the lowest values of "k" (1.11 and 2.71 10-3 min-1, respectively). It is noteworthy that this small variation in the value of k caused the half-life to decrease 2.4 times, from 624.5 min to 255.8 min with the use of UV-C light, which is more energetic. This is an indication that this material needs a higher energy to promote the electron from the valence band to the conduction band.

The TiO2-350-500 precursor also had an increased dye removal rate for UV-C light, a value of k=16.67 10-3 min-1 and a half-life of 41.6 min. This increase is also related to the band gap of the material.

Copper-doped nanomaterials were more effective in both UV-A and UV-C light, the presence of Cu II ion increased the removal speed, k value, in relation to the undoped material. Under UV-C light this increase is more evident, value of k= 87.92 10-3min-1.

Table 2

Comparing the results obtained with the literature, a greater efficiency of the materials synthesized by the route proposed in this work can be seen. Firstly, among materials without dopant and with the same crystalline structure, it was found that the rate constant of dye photodegradation under UV-C light irradiation was k= 9.50 10-3 min-1 while in this work it was of 55.40 10 -3 min -1.

Regarding the doped material, the percentage of methylene blue dye removal in 120 minutes of UV-A light irradiation for the doped ion exchange photocatalysts was 23% for the one containing sodium, 90% for the one containing Ag+ and 86% for the containing Cu2+ in the interlayer space. While in this work, the sample containing sodium removed 95.6% and the sample containing copper (obtained using the doped precursor) had a photocatalytic efficiency in UV-A light of 96.2% in just 60 minutes.

ANTIMICROBIAN ACTIVITY

The TiO2–350–500 sample showed

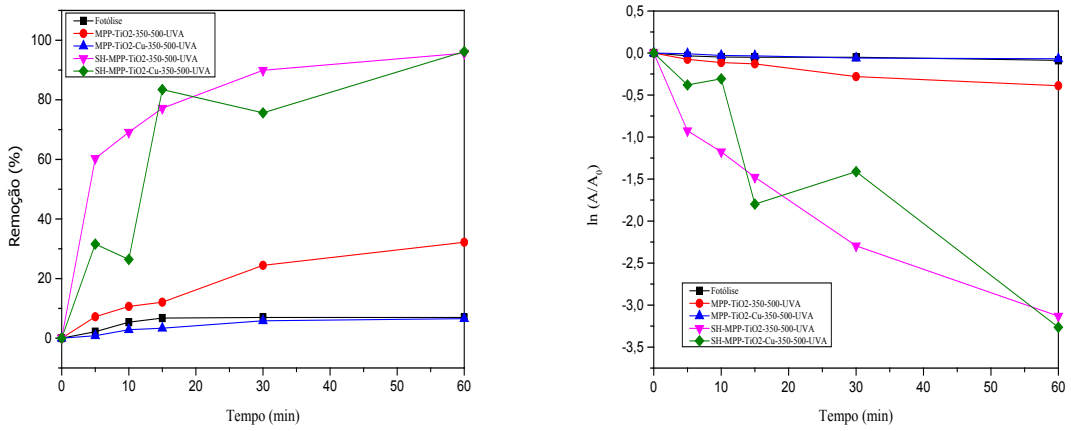

Figure 8 - Plot of %Methylene Blue Removal versus irradiation time and Pseudo first order kinetics model for the system, both under UV-A light.

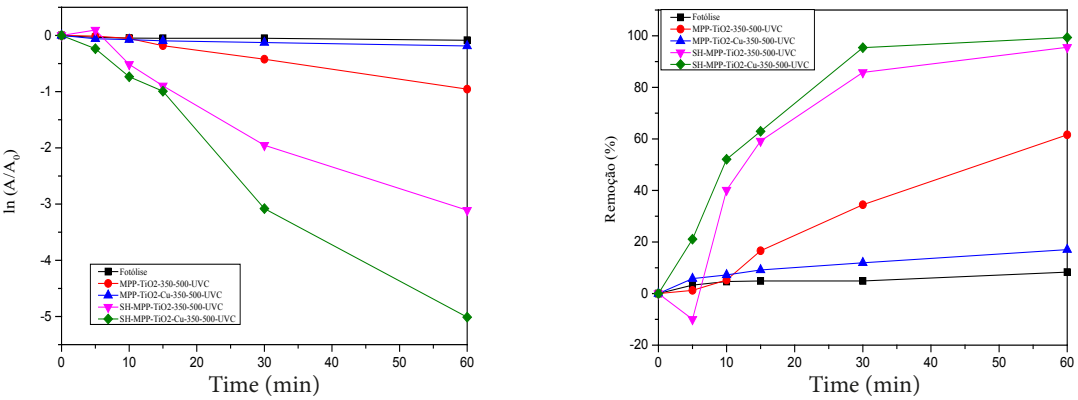

Figure 10 - Graph of %Methylene Blue Removal versus irradiation time and Pseudo first order kinetics model for the system, both under UV-C light.

Sample	Light	Removal Efficiency	Value of *k* (10^{-3} min^{-1})	R^2	$t_{1/2}$
TiO_2-350-500	UV-A	32,2%	6,31	0,93662	109,8
TiO_2-350-500-Cu	UV-A	6,6 %	1,11	0,78696	624,5
SH-TiO_2-350-500	UV-A	95,6 %	47,02	0,88204	14,7
SH-TiO_2-350-500-Cu	UV-A	96,2%	51,81	0,8353	13,4
TiO_2-350-500	UV-C	61,6%	16,67	0,9871	41,6
TiO_2-350-500-Cu	UV-C	17,1%	2,71	0,86556	255,8
SH-TiO_2-350-500	UV-C	95,5%	55,40	0,95784	12,5
SH-TiO_2-350-500-Cu	UV-C	99,3%	87,92	0,97462	7,9

Table 2: Comparison of velocity constant (k) according to each sample and radiated light energy.

Source: Author himself.

inhibition against the bacterium Enterococcus faecalis (gram positive) under the irradiation of black light (UV-A), it also showed inhibition against the strain Escherichia coli (gram negative) under the irradiation of UV-C light. However, for the sample doped with copper II, there was no antimicrobial activity.

The copper II-doped nanoparticle sample, obtained after hydrothermal synthesis, showed bactericidal activity against Staphylococcus aureus bacteria (gram positive) under black light irradiation (UV-A), and also against Bacilluscereus bacteria (gram positive) and Escherichia coli (gram negative) under UV-C light as copper is available for interactions.

The results of the antimicrobial test I and II are listed in Table 3 and Table 4.

Table 3 and 4

For these tests, irradiation of UV-A or UV-C light was used inside the bacteriological incubator during the entire incubation period, as the samples are "photoactivated". From these tests, and from the photocatalysis, it is verified that there is a greater facility to promote the electron from the Valencia layer (CV) to the conduction layer (CC) using UV-C light to irradiate the samples. It was also verified that the SH-TiO2–Cu-350–500 sample was more active in photocatalysis, a result that was repeated in the bactericidal test (sample partially sensitive to two strains of bacteria under UV-C light and one under UV-A light).

These tests give an indication that the copper (replacing the titanium atom in the center of the TiO6 octahedron) incorporated inside the crystal structure causes a distortion of the crystal lattice, because, in addition to being a larger ion, it decreases the number of bonds to the around it, thus being a more available site in the structure for oxidation/ reduction reactions.

CONCLUSION

The samples TiO2-350-500 ºC and TiO2-Cu-350-500 ºC showed 81.24% and 100% of anatase phase, respectively. Copper was added as a dopant and was incorporated into the crystal lattice of the material and, as indicated by Raman spectroscopy, replaced titanium in the center of the octahedron, a result evidenced by the shift of the peak from 147 cm-1 to 151 cm-1. These samples were active for photocatalysis in both UV-A and UV-C light. It was found that copper does not significantly improve the photocatalytic efficiency of the material.

After hydrothermal synthesis, the use of precursors containing copper in its structure made it possible to obtain the same type of nanostructure, layered titanates, and, due to the dissolution-reprecipitation process that occurs in the synthesis, it is inferred that the dopant is not trapped in the crystalline structure. The modification of the structure and morphology of these samples culminates in the improvement of photocatalytic efficiency (99.3% removal and k=87.92 10-3 min-1) and antimicrobial activity.

THANKS

The authors are grateful for the financial support to the CNPq project through the Universal project CNPQ- 422720/2016-0; the scientific initiation grant (PIBIC-UEMS) for the period 2015-2018; instrumental support CEPEMAT-Dourados-MS for the implementation of Raman measurements; and the scientific and instrumental support of prof. Dr. Maria Aparecida Zaghete IQ-Unesp-Araraquara-SP.

Samples	Bacteria		
	***S. aureous* (positive gram)**	***P. aeruginosa* (negative gram)**	***E. faecalis* (positive gram)**
TiO_2 – 350 – 500	Resistant	Resistant	Intermediary
TiO_2 – 350 – 500 – Cu	Resistant	Resistant	Resistant
SH - TiO_2 – 350 – 500	Resistant	Resistant	Resistant
SH - TiO_2 – 350 – 500 – Cu	Sensitive	Resistant	Resistant

Table 3: Results of the antimicrobial test using black light irradiation (UV-A).

Source: Author himself.

Samples	Bacteria		
	***E. faecalis* (positive gram)**	***E. coli* (negativegram)**	***B. cereus* (positive gram)**
TiO_2 – 350 - 500	Resistant	Parcialmente Sensitive	Resistant
TiO_2 – 350 – 500 – Cu	Resistant	Resistant	Resistant
SH - TiO_2 – 350 – 500	Resistant	Resistant	Resistant
SH - TiO_2 – 350 – 500 – Cu	Resistant	Intermediary	Intermediary

Table 4: Results of the antimicrobial test using UV-C light irradiation.

Source: Author himself.

REFERENCES

1 KUMAR,P., MAHAJAN, P., KAUR, R., GAUTAM, S., Nanotechnology and its challenges in the food sector: a review, **Materials Today Chemistry** 17 (2020) 100332.

2 YAMAGUCHI, Y.; SHIMODO, T.; USUKI, S.; TORIGOE, K.; TERASHIMA, C.; KATSUMATA, K.; IKEKITA, M.; FUJISHIMA, A.; SAKAIA, H.; NAKATA, K. Different hollow and spherical TiO2 morphologies have distinct activities for the photocatalytic inactivation of chemical and biological agents. **Photochemical & Photobiological Sciences**, 15, (2016) 988–994.

3 NAKANO, R.; ISHIGURO, H.; YAO, Y.; KAJIOKA, J.; FUJISHIMA, A.; SUNADA, K.; MINOSHIMA, M.; HASHIMOTOD, K.; KUBOTA, Y. Photocatalytic inactivation of influenza virus by titanium dioxide thin film. **Photochemical & Photobiological Sciences**. 11, (2012), 1293- 1298.

4 ISHIGURO, H.; YAO, Y.; NAKANO, R.; HARA, M.; SUNADA, K.; HASHIMOTO, K.; KAJIOKA, J.; FUJISHIMA, A.; KUBOTA, Y. Photocatalytic activity of Cu2+/TiO2-coated cordierite foam inactivates bacteriophages and Legionella pneumophila. **Applied Catalysis B: Environmental**, 129, (2013) 56– 61.

5 NAKANO, R.; HARA, M.; ISHIGURO; H.; YAO, Y.; OCHIAI, T.; NAKATA, K.; MURAKAMI, T.; KAJIOKA, J.; SUNADA, K.; HASHIMOTO, K.; FUJISHIMA, A.; KUBOTA, Y. Broad Spectrum Microbicidal Activity of Photocatalysis by TiO2. **Catalysts**, 3, (2013) 310-323.

6 HASHIMOTO, K.; IRIE, H.; FUJISHIMA, A.TiO2 Photocatalysis: A Historical Overview and Future Prospects. **Japanese Journal of Applied Physics**, 44, 12, (2005) 8269–8285.

7 KASUGA, T.; HIRAMATSU, M.; HOSON, A.; SEKINO, T.; NIIHARA, K. Formation of titanium oxide nanotube. **Langmuir**, 14, (1998) 3160-3163.

8 MANFROI, D. C.; ANJOS, A. dos; CAVALHEIRO, A. A.; PERAZOLLI, L. A.; VARELA, J. A.; ZAGHETE, M. A. Titanate nanotubes produced from microwave-assisted hydrothermal synthesis: photocatalytic and structural properties. **Ceramics International**, 40, (2014) 14483-14491.

9 SCHERRER, V. P. Bestimmung der InnerenStruktur und der Größe von Kolloidteilchen Mittels Röntgenstrahlen. **Göttinger Nachrichten Math. Phys**., 2, (1918) 98– 100,

10 DE OLIVEIRA, R. R. Estudo do efeito da tensão residual na microdeformação da rede cristalina e no tamanho de cristalito em aço Cr-Si-V jateado com granalhas de aço (TESE), **INSTITUTO DE PESQUISAS ENERGÉTICAS E NUCLEARES**, São Paulo, 2016.

11 HABIBA, U.; SHARIFULISLAM, MD.; SIDDIQUE, T. A.; AFIFI, AMALINA M.;ANG, B. C.Adsorption and photocatalytic degradation of anionic dyes on Chitosan/PVA/Na–Titanate/TiO2composites synthesized by solution casting method. **Carbohydrate Polymers**, 149 (2016) 317-331.